



**HAL**  
open science

## Small-Molecule 3D Ligand for RNA Recognition: Tuning Selectivity through Scaffold Hopping

Simon Felder, Corinne Sagné, Erica Benedetti, Laurent Micouin

► **To cite this version:**

Simon Felder, Corinne Sagné, Erica Benedetti, Laurent Micouin. Small-Molecule 3D Ligand for RNA Recognition: Tuning Selectivity through Scaffold Hopping. ACS Chemical Biology, 2022, 17 (11), pp.3069-3076. 10.1021/acscchembio.2c00171 . hal-04035021

**HAL Id: hal-04035021**

**<https://hal.science/hal-04035021v1>**

Submitted on 17 Mar 2023

**HAL** is a multi-disciplinary open access archive for the deposit and dissemination of scientific research documents, whether they are published or not. The documents may come from teaching and research institutions in France or abroad, or from public or private research centers.

L'archive ouverte pluridisciplinaire **HAL**, est destinée au dépôt et à la diffusion de documents scientifiques de niveau recherche, publiés ou non, émanant des établissements d'enseignement et de recherche français ou étrangers, des laboratoires publics ou privés.

# Small-molecule 3D ligand for RNA recognition: tuning selectivity through scaffold hopping

Simon Felder,<sup>a</sup> Corinne Sagné,<sup>b</sup> Erica Benedetti,<sup>a,\*</sup> and Laurent Micouin<sup>a,\*</sup>

<sup>a</sup> Université de Paris, CNRS, Laboratoire de Chimie et de Biochimie Pharmacologiques et Toxicologiques, F-75006 Paris, France.

[erica.benedetti@u-paris.fr](mailto:erica.benedetti@u-paris.fr) ; [laurent.micouin@u-paris.fr](mailto:laurent.micouin@u-paris.fr);

<sup>b</sup> Université de Paris, CNRS, Saints-Pères Paris Institute for the Neurosciences, F-75006 Paris, France

---

**ABSTRACT:** Targeting RNAs with small molecules is considered the next frontier for drug discovery. In this context, the development of compounds capable of binding RNA structural motifs of low complexity with high affinity and selectivity would greatly expand the number of targets of potential therapeutic value. In this study, we demonstrate that tuning the three-dimensional shape of promiscuous nucleic acid binders is a valuable strategy for the design of new selective RNA ligands. Indeed, starting from a known cyanine, the simple replacement of a phenyl ring with a [2.2]paracyclophane moiety led to a new compound able to discriminate between nucleic acids showing different structural characteristics with a marked affinity and selectivity for an octahairpin loop RNA sequence. This shape modification also affected the *in cellulo* behavior of the cyanine. These results suggest that scaffold hopping is a valuable strategy to improve the selectivity of RNA/small-molecule interactions and highlight the need to explore new chemical space for the design of selective RNA ligands.

---

## INTRODUCTION

The recognition of the importance of RNA regulatory role in cell homeostasis as well as the increasing evidence of its implication in many diseases has led to a growing interest in targeting RNA as a new strategy in medicinal chemistry.<sup>1-7</sup> To reach this goal, two main approaches can be envisaged, considering RNA either as a sequence of nucleotides or as a structured biomolecule. The first approach has led to the development of antisense oligonucleotides (ASO), several of which are nowadays available on the market.<sup>8,9</sup> However, a sequence-based RNA recognition strategy usually requires the design of highly charged compounds with multiple hydrogen bond donors or acceptors and physicochemical properties known to lead to *in-vivo* delivery problems.<sup>10</sup> The second approach aims at targeting RNA structured regions with drug-like small molecules. This method has only recently proved successful, the first example of a drug interacting with non-ribosomal RNA being approved only recently.<sup>11</sup> However, despite the important progress achieved in understanding the structural requirements for the design of drug-like compounds with strong affinity towards RNA, guidelines to improve the selectivity of RNA/small-molecule interactions are still to be defined.<sup>6,12-14</sup>

As a matter of fact, most of the advanced active compounds currently under study in preclinical and clinical trials have been elaborated starting from phenotypic assays, a technique that may entail complex target deconvolution. One way to avoid this issue is to directly select

relevant targets that possess known highly-structured binding pockets of important complexity to facilitate specific recognition.<sup>6</sup> Nonetheless, although this approach is very promising, many potential targets of interest can include RNA secondary motifs of low complexity, such as bulges or stem loops. Targeting these structures with a good selectivity is therefore a challenging, but important goal to expand the space of druggable RNAs.

This difficult problem has been addressed in two different ways up to now. The first method consists in combining diverse RNA-binding fragments using appropriate linkers to preferentially interact with hairpin loops of a given size<sup>15,16</sup> or be able to discriminate between different transfer RNAs.<sup>17,18</sup> When combined with multivalency, this strategy can indeed deliver compounds with excellent affinities and a good selectivity towards internal loops.<sup>19</sup> The second, less investigated strategy, consists in exploring the chemical space to escape the rod-like or flat molecules generally considered to be privileged structures for the design of RNA binders.<sup>14</sup> This approach led to the development of wedge-shaped compounds,<sup>20</sup> cylinders<sup>21,22</sup> or tryptices<sup>23,24</sup> bearing non coplanar aromatic moieties capable of interacting with RNA secondary structures through  $\pi$ -stacking, while at the same time avoiding promiscuous intercalation or groove binding (Figure 1). Inspired by these pioneering examples, we decided to investigate the possibility to improve the selectivity of RNA binders by incorporating unusual 3D elements onto their structure.

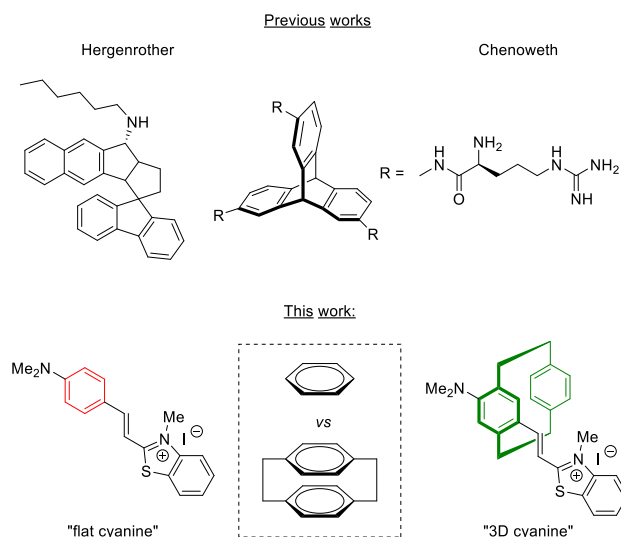


**Figure 1.** Examples of RNA binders bearing non-coplanar aromatic moieties

In particular, we envisaged replacing their “flat” aromatic rings with a [2.2]paracyclophane (pCp) unit whose unique three-dimensional shape is well-known (Figure 2).<sup>25–27</sup> Taking into consideration the distance between the two aromatic rings of this compound (3.04 Å) and the helical rise per base pair of double-stranded RNA (2.6 Å) or DNA (3.4 Å) (Figure 2),<sup>28</sup> we assumed that the pCp scaffold should not intercalate between two base pairs. This motif could therefore serve as building block to develop new compounds able to interact preferentially with nucleic acids incorporating single-stranded regions.

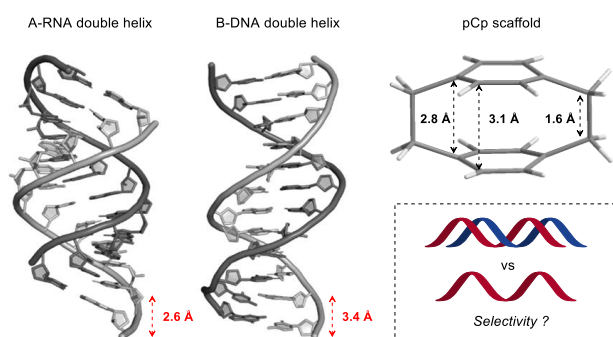


**Figure 2.** Structural characteristics of pCp, A-RNA double helix, and B-DNA double helix

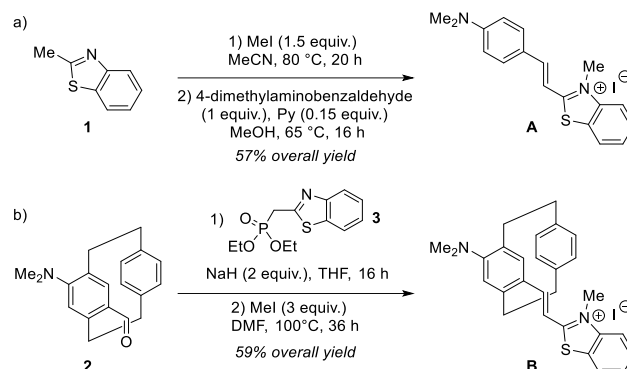
In this proof of concept study, we describe the synthesis of an unprecedented cyanine dye (Figure 1). Starting from a general planar nucleic acid binder and following a scaffold hopping strategy,<sup>29</sup> we demonstrate that the simple replacement of a phenyl ring with a [2.2]paracyclophane moiety leads to a new compound capable of discriminating between nucleic acids showing different structural characteristics with a marked affinity and selectivity for an octahairpin loop RNA sequence. We finally show that this shape modification also affects the *in cellulo* behaviour of the dyes.

## RESULTS AND DISCUSSION

### Synthesis and characterization of the cyanine dyes

Cyanine **A** was chosen as a model substrate because of its known ability to show a significant fluorescence enhancement upon binding to nucleic acids.<sup>30–32</sup> This compound was synthesized in two steps according to previously reported procedures in 57% overall yield (Scheme 1a). The pCp-based three-dimensional analogue **B** was then prepared in two steps, starting from key intermediate **2**<sup>33</sup> in 59% yield (Scheme 1b).

### Scheme 1. Synthesis of cyanines **A** and **B**



The spectroscopic properties of compounds **A** and **B** were studied in dichloromethane and in TE [TRIS (10 mM) and EDTA (1 mM) buffer, pH 7.4]. In both organic and aqueous solutions, the flat dye **A** exhibited intense absorption bands in the green region of the electromagnetic spectrum (Table 1). The absorption maxima of the pCp-based dye **B** were significantly red-shifted in comparison with those of cyanine **A** (yellow region, Table 1).<sup>34–35</sup> This behaviour is certainly due to the presence of the pCp moiety, which can be considered as a mild electron-donating group. Analogous bathochromic shifts were observed in emission. In this case, clear fluorescence bands could be recorded for both dyes in  $\text{CH}_2\text{Cl}_2$  at 597 nm and 640 nm respectively (Table 1). However, as expected, a significant fluorescence quenching was detected in aqueous solutions ( $\phi_f < 0.1\%$ , Table 1).

**Table 1.** Spectroscopic properties of compounds **A** and **B**

Dye <sup>[a]</sup>	Solvent	$\lambda_{\text{abs}}^{\text{max}}$ (nm)	$\epsilon_{\text{max}}$ ( $\text{M}^{-1}\cdot\text{cm}^{-1}$ )	$\lambda_{\text{em}}^{\text{max}}$ (nm)	$\phi_f$ (%)
<b>A</b>	$\text{CH}_2\text{Cl}_2$	553	89600	597	1.8 <sup>[b]</sup>
	TE	510	37600	595	<0.1
<b>B</b>	$\text{CH}_2\text{Cl}_2$	596	54400	640	2.3 <sup>[c]</sup>
	TE	565	33800	630	<0.1

[a]  $10^{-5}$  M solutions. [b] The fluorescence quantum yield of cyanine **A** in  $\text{CH}_2\text{Cl}_2$  was reported previously, see ref. 36. [c] The relative fluorescence quantum yield of cyanine **B** in  $\text{CH}_2\text{Cl}_2$  was determined by using crystal violet as a standard ( $\phi_f = 1.9\%$  in glycerol).

## Fluorescence enhancement studies

Having the cyanines in hand, we first investigated the behaviour of compound **B** in the presence of Baker's yeast total RNA (*S. cerevisiae*), mainly containing rRNA. To our delight, the three-dimensional pCp-based cyanine displayed a significant turn-on fluorescence response. Indeed, a titration performed by adding increasing quantities of RNA (0 to 2 mg) to a 1  $\mu$ M solution of dye **B** in TE led to a 30-fold intensity enhancement (Figure 3). X-ray analysis of the pCp-derived cyanine shows an interesting "head-to-toe" crystal packing pattern (Figure S8), and NMR experiments performed in CD<sub>2</sub>Cl<sub>2</sub> at different concentrations suggest the formation of multimers in solution (Figures S5 and S6). The observed fluorescence enhancement of dye **B** is therefore supposed to arise from disaggregation processes occurring upon monomer interaction with the nucleic acid.<sup>37</sup> RNA digestion assays confirmed that the increased emissions originate only from the presence of RNA in solution, as a rapid fluorescence "turn-off" was observed upon treatment with ribonuclease (RNase A, Figures S10-S13).

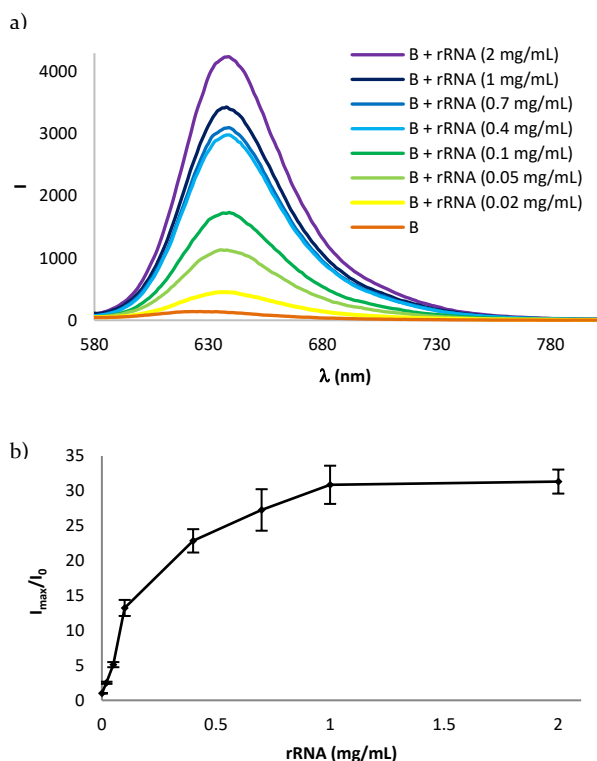


**Figure 3.** (a) Representative fluorescence titration of pCp-based cyanine **B** with increasing quantities of Baker's yeast RNA in a TE at 20 °C. (b) Plot of fluorescence intensity enhancement ( $I_{\max}/I_0$ ,  $\lambda_{\text{ex}} = 550$  nm) in the presence of increasing quantities of Baker's yeast RNA (0 to 2 mg/mL). Data are presented as mean of the three independent experiments (error bar: standard deviation).

Encouraged by these findings, we undertook a selectivity study, and compared the fluorescence responses of the three-dimensional pCp cyanine **B** with those of the flat dye **A** in the presence of various nucleic acids. Fluorescence titration of both compounds with tRNA (from

baker's yeast, *S. cerevisiae*), DNA (from calf thymus), dsRNA (5'-3': CCAGUUCGUAGUAACCC), and ssRNA (5'-3': UUGUACUACACAAAAGUACUG) revealed quite divergent behaviours. In fact, while similar fluorescence enhancements were observed for dye **A** in all cases, the response of the three-dimensional cyanine **B** was found to strongly depend on the nature of the nucleic acid with which it interacts (Figure 4). While only moderate fluorescence enhancements were obtained in the presence of DNA and double stranded RNA, increased emission similar to those described above for total RNA were observed with single stranded RNA. Cyanine **B** exhibited its strongest response in the presence of tRNA (up to 40-fold with the addition of 0.4 mg/mL of nucleic acid). The fluorescence enhancement, in this case, is comparable to that achieved with the flat dye **A**. As tRNA, rRNA and DNA are total nucleic acid extracts of different sequences, three independent experiments at different concentrations (0.4 mg/mL and 2 mg/mL) were performed to ensure the reproducibility of the results (see the SI for more details). These evidences support our hypothesis that tuning the three-dimensional shape of a flat molecule is a viable strategy to turn a promiscuous nucleic acid binder into a new selective ssRNA ligand.

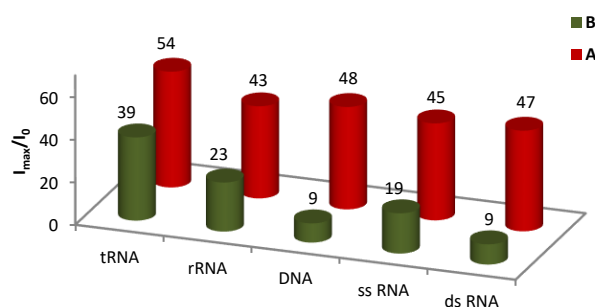


**Figure 4.** Selectivity of cyanines **A** or **B** ( $10^{-6}$  M) versus different species of nucleic acids (0.4 mg/mL) in a TE at 20 °C. Mean values of three independent experiments are reported in the graphic for tRNA, rRNA and DNA (see the SI for more details).

Indeed, the moderate fluorescence enhancements observed with DNA and dsRNA attest that the cyanine **B** tends to interact poorly with nucleic acids showing a double helical structure. On the other hand, tRNA and rRNA incorporate several single-stranded regions. The different fluorescence response detected in the presence of these nucleic acids may arise from the diverse percentage of unpaired bases statistically found in tRNA and rRNA (36% and 26% respectively).<sup>38</sup> The structure characteristics and accessibility of these regions may also play an important role in the dynamics of the interactions. Finally, while the chosen ssRNA is known to show no preferential secondary structure, we cannot exclude the possibility of an induced-fit in the presence of dye **B**. The occurrence of such an event may influence the fluorescence intensity variations observed in the presence of this RNA sequence.

Photobleaching studies were performed in the presence of tRNA. The fluorescence emission of both cyanines **A** and **B** with this nucleic acid proved to be stable over the time at 20 °C (Figure 5).<sup>39,40</sup>

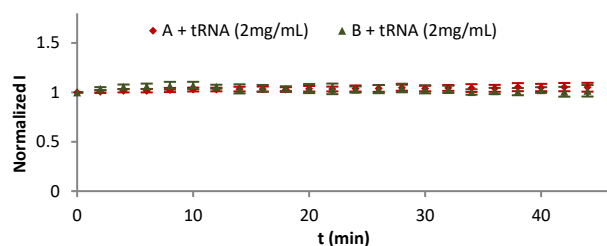
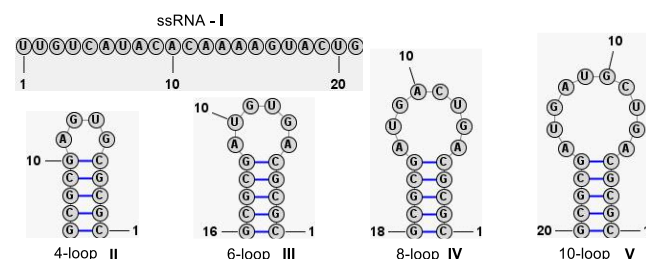


**Figure 5.** Photobleaching studies.  $10^{-6}$  M solutions of cyanine **A** + tRNA (2 mg/mL) in TE ( $\lambda_{\text{ex}} = 500$  nm;  $\lambda_{\text{max}} = 600$  nm) or **B** + tRNA (2 mg/mL) in TE ( $\lambda_{\text{ex}} = 550$  nm;  $\lambda_{\text{max}} = 625$  nm). The samples were continuously irradiated for 45 min at 20 °C, and maximum emission intensity changes were measured at 2-minute time intervals. Data are presented as mean of the three independent experiments (error bar: standard deviation).

### Selective interactions with hairpin loop RNA structures

We next set-up to investigate whether the pCp-based cyanine **B** could exhibit different behaviours in the presence of structured ssRNA sequences of various sizes. To this end, fluorescence titrations were employed to evaluate the interaction of cyanine **B** with previously reported tetra-, hexa-, octa- and decahairpin loop structures (**II-V**, Table 2).<sup>15</sup> Note that the decaloop **V** used thereafter was designed starting from the octaloop sequence **IV**, and no privileged structures other than a hairpin could be predicted for this oligonucleotide. Interestingly, the pCp-based compound showed a strong affinity and good selectivity towards large loops, with a preference for the octaloop sequence **IV**.

**Table 2.** Dissociation constants ( $K_d$ ,  $\mu\text{M}$ ) for RNA/cyanine **B** interactions



I[a]	II [a]	III[a]	IV[b]	IV[c]	V[b]
14.22	24.53	6.04	0.54	1.18	1.65
$\pm 14.46$	$\pm 6.60$	$\pm 2.05$	$\pm 0.16$	$\pm 0.04$	$\pm 1.14$

[a]  $10^{-6}$  M solutions of dye **B** in TE. [b]  $10^{-7}$  M solutions of dye **B** in TE [c]  $10^{-7}$  M solutions of dye **B** in TE supplemented with 100 mM KCl, and 2 mM  $\text{MgCl}_2$ . Data are presented as mean of the three independent experiments  $\pm$  standard deviation.

The  $K_d$  value ( $0.54 \mu\text{M}$ , Table 2) observed with this oligonucleotide is indeed  $\sim 3$ -fold lower than the one determined in the presence of the decahairpin loop **V**,  $11$ -fold lower than the one obtained with the hexaloop **III**, and up to  $45$ -fold lower than the values calculated for the tetraloop sequences **II** (Table 2). Cations are known to strongly bind to RNA because of electrostatic interactions with the phosphodiester backbone. Such interactions are important to achieve high affinities but are also responsible for promiscuous binding. On the other hand, hydrogen bonding or  $\pi$ -stacking interactions can only happen in pre-arranged regions presenting appropriate chemical moieties, thus bringing selectivity to the recognition.<sup>41</sup> Compound **B** is positively charged and presents an extended  $\pi$ -conjugated system. The pCp-based cyanine can thus bind to RNA through electrostatic interactions as well as aromatic stacking. We therefore decided to perform a fluorescence titration in a salt supplemented buffer (TE with 100 mM KCl, and 2 mM  $\text{MgCl}_2$ ) to minimize the electrostatic determinant while maintaining the structure-based  $\pi$ -stacking as the main source of affinity. In the presence of salts, the dissociation constant measured for dye **B** with the octaloop sequence **IV** was only  $\sim 2.5$ -fold higher than the one measured in the salt deprived buffer (value in bold, Table 2). This result suggests that electrostatic interactions have little influence over the association between cyanine **B** and RNA. All these studies were conducted with the racemic cyanine **B**. Note that the two enantiomers of this molecules were also prepared separately and exhibited similar affinity for the 8-loop **IV** ( $R_p$ -**B**:  $K_d = 0.93 \pm 0.12 \mu\text{M}$ ;  $S_p$ :  $K_d = 0.75 \pm 0.22 \mu\text{M}$ ). Chemical<sup>42-44</sup> and thermal denaturation assays were finally realized.

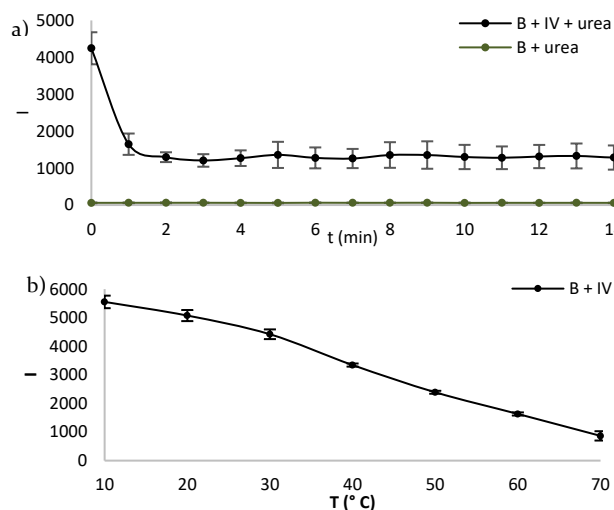


**Figure 6.** RNA denaturation assays: a) Cyanine **B** ( $10^{-6}$  M in TE), alone or in the presence of **IV** ( $10 \mu\text{M}$ ) was treated with urea ( $2\text{M}$ ). Fluorescence emission ( $\lambda_{\text{ex}} = 550$  nm,  $\lambda_{\text{max}} = 640$  nm) was measured at 1-minute time intervals for 15 minutes at 20 °C. b) Cyanine **B** ( $10^{-6}$  M in TE) in the presence of **IV** ( $10 \mu\text{M}$ ) was progressively heated from 10 to 70 °C. The fluorescence emission ( $\lambda_{\text{ex}} = 550$  nm,  $\lambda_{\text{max}} = 640$  nm) was recorded every 10 °C. Data are presented as mean of three independent experiments (error bar: standard deviation).

These experiments (Figure 6) highlighted that the increased emission of cyanine **B** observed in the presence of the octahairpin loop **IV**, and therefore its affinity and selectivity, originate from the presence of structured RNA in solution. A fluorescence “turn-off” response was indeed observed upon treatment with urea or while heating the samples up to 70 °C. Note that, in the case of thermal denaturation, the original fluorescence intensity was recovered when the sample was cooled back to 10 °C.

### In cellulo imaging

We lastly performed epifluorescence microscopy experiments with HeLa cells to study the behaviour of cyanines **A** and **B** *in cellulo*. Live cells incubated with compound **A** at a concentration of 1  $\mu\text{M}$  displayed fluorescence in the nucleoli and cytoplasm (Figure 7a). Time dependent fluorescence intensity and localisation were observed during the experiment in the presence of dye **A**, as the nucleolar staining became more intense within seconds of light exposure (see Figure S15 for more details). This behaviour has previously been associated to cellular phototoxicity of cyanine **A**.<sup>39,40</sup>

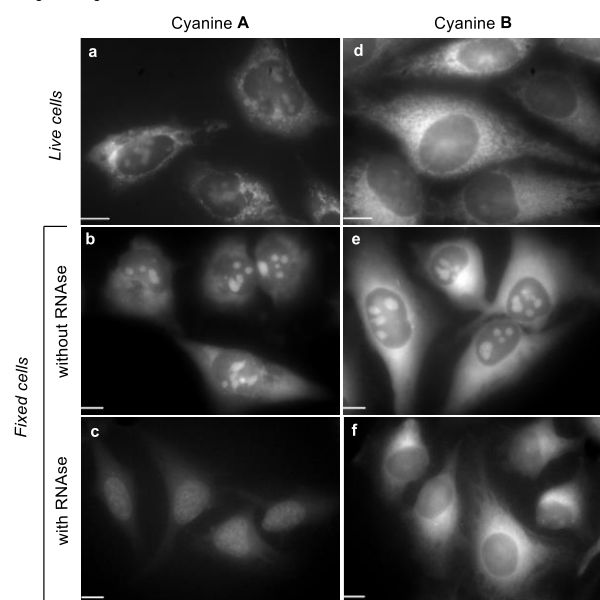


**Figure 7.** *In cellulo* imaging experiments. HeLa cells incubated with cyanine **A** [1  $\mu\text{M}$  (a) or 5  $\mu\text{M}$  (b and c)] or cyanine **B** [5  $\mu\text{M}$  (d-f)] for 20 min. Fixed cells were imaged after 2 h of incubation at 37 °C without (b and e) or with RNase (c and f). Scale bar = 10  $\mu\text{m}$ .

On the contrary, live cells incubated with the pCp-based cyanine **B** at a concentration of 5  $\mu\text{M}$  mainly showed a cytoplasmic fluorescence, with a peculiar perinuclear staining (possibly the ER region, Figure 7d). Compared to **A**, the nucleolar staining of dye **B** in live cells appeared less noticeable. This behaviour is possibly due to the fact that the pCp-based cyanine does not penetrate easily into the cell nucleus or is readily removed by active transport processes. In this case, the cell labelling remained stable after exposure to light irradiation over several minutes, thus suggesting a reduced phototoxicity of dye **B** in comparisons with **A** *in cellulo*.

In fixed cells, a similar cytoplasmic and nucleolar labelling was observed for both dyes, although the unusual marked perinuclear fluorescence was again detected in the presence of the pCp-based cyanine **B** (Figure 7b and 7e). However, digestion experiments with ribonuclease revealed a very different behaviour of the dyes. Indeed, upon treatment with RNase **A**, cells previously incubated with cyanine **A** displayed an almost exclusive nuclear staining (Figure 7c).<sup>45</sup> On the contrary, for the cells incubated with cyanine **B** and treated with RNase **A**, only the nucleolar staining disappeared, while the cytoplasmic labelling was retained (Figure 7f). No nuclear fluorescence was detected in this case, thus confirming the poor affinity of the three-dimensional cyanine towards DNA in cells.

### Conclusions

In summary, in this proof of concept study, we have shown that it is possible to tune the selectivity of a “flat” promiscuous fluorescent nucleic acid binder using a scaffold hopping strategy.<sup>29</sup> Indeed, the simple replacement of the central phenyl group of a cyanine dye with a [2.2]paracyclophane moiety led to a new compound able to discriminate between nucleic acids showing different structural characteristics. The three-dimensional dye was found capable of binding to an RNA octaloop with a high degree of selectivity over other “smaller” loop sizes. Imaging experiments confirmed that this shape modification can also affect the *in cellulo* behaviour of the RNA binders. This work illustrates the power of a scaffold hopping strategy to explore new chemical spaces for the design of selective RNA binders. It also outlines that compounds bearing non-coplanar aromatic moieties such as the pCp scaffold can be considered as valuable privileged motives to target RNA secondary structures with marked selectivity.

### METHODS

#### Chemical synthesis

All reactions were carried out under inert atmosphere, (in oven-dried glassware, using dry solvents) unless otherwise specified. All commercially available compounds were purchased from Aldrich Chemical Co., Acros Organics or Ugarit, and used as received. Analytical thin layer chromatography (TLC) was performed on silica gel plates (Merck 60F254) visualized with a UV lamp (254 nm). Flash chromatography was performed on silica gel (60-230 mesh) unless otherwise specified. Organic extracts were dried over anhydrous  $\text{MgSO}_4$ . NMR spectra ( $^1\text{H}$  and  $^{13}\text{C}\{^1\text{H}\}$ ) were recorded on Bruker Avancell 500 spectrometer, at 500 MHz ( $^1\text{H}$  value) in  $\text{CDCl}_3$ ,  $\text{CDCl}_2$  or  $\text{DMSO-d}_6$ . Spectra were referenced to residual non-deuterated solvent signal (chloroform: 7.26 ppm,  $^1\text{H}$ ; 77.0 ppm,  $^{13}\text{C}\{^1\text{H}\}$ ; dichloromethane: 5.32 ppm,  $^1\text{H}$ ; 53.84 ppm,  $^{13}\text{C}\{^1\text{H}\}$ ; dimethylsulfoxide: 2.50 ppm,  $^1\text{H}$ ; 39.52 ppm,  $^{13}\text{C}\{^1\text{H}\}$ ). Chemical shifts are reported in ppm, multiplicities are indicated by s (singlet), d (doublet), t (triplet), q (quartet), p (pentet), and m (multiplet or overlap of nonequivalent resonances), dd (doublet of doublet), td (triplet of doublet), and br (broad signal). Coupling constants, J, are reported in hertz (Hz). DEPT-135 experiments were used to assign  $^{13}\text{C}$

NMR spectra. All NMR spectra were obtained at 300K unless otherwise specified. IR spectra were obtained using a spectrum one FT-IR spectrometer (Perkin Elmer). Optical rotations ( $\alpha_D$ ) were measured on a Perkin Elmer polarimeter (model 341) at 20 °C. Absorption and fluorescence spectra were recorded on UV-2700 spectrophotometer (Shimadzu) and F-7000 fluorescence spectrometer (Hitachi), respectively. The photophysical characterization of the products was performed at 20 °C, on air-equilibrated solutions, using quartz cuvettes with 1 cm optical path length.

### Fluorescence enhancement studies

Fluorescence spectra were recorded on a F-7000 fluorescence spectrometer (Hitachi). The photophysical measurements were performed at 20 °C on air-equilibrated solutions, using quartz cuvettes with 1 cm optical path length.  $10^{-6}$  M solutions of cyanine dyes **A** or **B** in TE buffer were used to perform the studies ( $\lambda_{exA} = 500$  nm;  $\lambda_{exB} = 550$  nm). Dyes concentration was kept constant during the titrations. tRNA (Roche, from baker's yeast, *S. cerevisiae*), DNA (from calf thymus), and total RNA (from baker's yeast, *S. cerevisiae*) were purchased from Sigma-Aldrich. ssRNA (5'-3': UUGUCAUACACAAAAGUACUG), and ds RNA (5'-3': CCAGUUCGUAGUAACCC) were purchased from Eurogentec. All nucleic acids were dissolved in an appropriate amount of TE buffer at pH 7.4 and left to fully hydrate over night at 4 °C. The TE buffer (Tris EDTA buffer, 10 mM and 1 mM respectively) was freshly prepared the day before the analysis using RNase-free water. Concentrations of all nucleic acids were calculated from measured  $A_{260}$  of diluted stock solutions based on the assumption that  $A_{260} = 1$  corresponds to a concentration of 40 or 50  $\mu\text{g}/\text{mL}$  of RNAs or DNA respectively.

### X-ray crystallography

A single crystal of compound **B** was selected, mounted onto a cryoloop, and transferred in the cold nitrogen gas stream of an Oxford Cryostream. Intensity data were collected with a BRUKER Kappa-APEXII diffractometer with micro-focused Cu-K $\alpha$  radiation ( $\lambda=1.54178$  Å) at 200K. APEX 3 suite and SAINT program (BRUKER) were used to carry out data collection, unit-cell parameters refinement, integration and data reduction. SADABS (BRUKER) was used for scaling and multi-scan absorption corrections. In the Olex2 suite<sup>46</sup>, the structure was solved with SHELXT-14<sup>47</sup> program and refined by full-matrix least-squares methods using SHELXL-14<sup>48</sup>. All non-hydrogen atoms were refined anisotropically. Hydrogen atoms were placed at calculated positions and refined with a riding model. CCDC 2123610 contains the supplementary crystallographic data for this paper. The data can be obtained free of charge from The Cambridge Crystallographic Data Centre via [www.ccdc.cam.ac.uk/structures](http://www.ccdc.cam.ac.uk/structures)

### Determination of the dissociation constants

10-loop (5'-3': CGCGCAGUCGUAGUAGCGCG, **V**), 8-loop (5'-3': CGCGCAGUCAGUAGCGCG, **IV**), 6-loop (5'-3': CGCGCAGUGUAGCGCG, **III**), 4-loop (5'-3': CGCGCAGUGAGCGCG, **II**), ssRNA (5'-3': UUGUCAUACACAAAAGUACUG, **I**) were purchased from Euro-

gentec. All assays were performed at 20 °C, by incremental addition of appropriately diluted nucleic acid solutions with 2 min equilibration time in between each measurement. Dye solutions were obtained by dilution from a 250  $\mu\text{M}$  stock solution in TE buffer. Nucleic acids were dissolved in 1 mL of TE buffer – concentrations are in the range of 0.5 mM to 1 mM depending on exact amounts provided by manufacturers – and kept at 4 °C overnight for complete hydration, then heat denatured (2 min at 95 °C), immediately placed in ice for 15 min, and warmed-back to rt over 15 min prior to use and conserved frozen after. All dilutions for all independent experiments were performed from these stock solutions. The volume of the increments was kept minimal to avoid excessive dilutions. All Kd calculations were performed using the bindfit program from [supramolecular.org](http://supramolecular.org), including dilution correction, in a 1:1 hypothetical binding model (<http://supramolecular.org>)<sup>49,50</sup>. Dissociation constants provided are the average of two independent experiments.

### In cellulo imaging

HeLa cells were cultured in EMEM medium supplemented with 1% non-essential amino acids, 10% FBS, 50U·mL<sup>-1</sup> penicillin, and 50  $\mu\text{g}\cdot\text{mL}^{-1}$  streptomycin at 37 °C and 5% CO<sub>2</sub>. Twenty-four hours before experiments, 50000 cells per well were plated onto glass coverslips in 24-well plates. Cells were briefly washed two times with PBS supplemented with 0.1 mM CaCl<sub>2</sub> and either labeled directly with RNA probes for "live cells", or treated for 30 min at room temperature with 4% PFA in PBS and permeabilized during 5 min with 0.1% Triton X-100 for "fixed cells". Cells were incubated for 20 min with solutions of either dye **A** (1 or 5  $\mu\text{M}$ ) or **B** (5 or 10  $\mu\text{M}$ ) in TE buffer alone for "fixed cells", or supplemented with 140 mM NaCl, 4 mM KCl, 2.5 mM CaCl<sub>2</sub>, 1 mM MgCl<sub>2</sub> for "live cells". For RNase treatment, labeled fixed cells were incubated for 2h in 500  $\mu\text{L}$  of buffer supplemented or not with 150  $\mu\text{g}\cdot\text{mL}^{-1}$  of RNase A. In all cases, labeled cells were imaged immediately with a Nikon Eclipse TE-2000 microscope equipped with a CCD camera (Coolsnap).

### ASSOCIATED CONTENT

The supporting information is available free of charge via the Internet at <http://pubs.acs.org>.

Details of experimental procedures including the synthesis of enantiopure **B**, UV-vis and fluorescence spectra, representative examples of the titration assays, URL's of all the fits, photobleaching studies, *in cellulo* imaging and RNase digestion experiments, <sup>1</sup>H NMR and <sup>13</sup>C NMR spectra (PDF).

### AUTHOR INFORMATION

#### Corresponding Author

**Laurent Micouin** - Université de Paris, CNRS, Laboratoire de Chimie et de Biochimie Pharmacologiques et Toxicologiques, F-75006 Paris, France ; [orcid.org/0000-0003-1080-8591](http://orcid.org/0000-0003-1080-8591) ; Email : [laurent.micouin@u-paris.fr](mailto:laurent.micouin@u-paris.fr)

**Erica Benedetti** - Université de Paris, CNRS, Laboratoire de Chimie et de Biochimie Pharmacologiques et Toxicologiques, F-75006 Paris, France ; orcid.org/0000-0002-6457-7381 ; Email : [erica.benedetti@u-paris.fr](mailto:erica.benedetti@u-paris.fr)

## Authors

**Simon Felder** - Université de Paris, CNRS, Laboratoire de Chimie et de Biochimie Pharmacologiques et Toxicologiques, F-75006 Paris, France

**Corinne Sagné** - Université de Paris, CNRS, Saints-Pères Paris Institute for the Neurosciences, F-75006 Paris, France

## Author Contributions

The manuscript was written through contributions of all authors.

## Notes

The authors declare no competing financial interest.

## ACKNOWLEDGMENT

We gratefully thank the CNRS, Université de Paris and the MESRI for financial support. L.-M. Chamoreau (Plateforme Diffraction X, IPCM, Sorbonne Université) and P. Gerardo (Plateforme de spectrométrie de masse, LCBPT, Université de Paris) are kindly acknowledged for their assistance with X-ray crystallography and mass analysis. We are grateful to N. Vanthuyne (iSm2, Aix-Marseille Université) for his assistance with chiral HPLC. We thank H. Mimouni and I. Fanget for help with cell cultures and analysis, and B. Colasson for fruitful discussions.

## ABBREVIATIONS

RNA, ribonucleic acid; DNA, deoxyribonucleic acid; ASO, antisense oligonucleotides; rRNA, ribosomal ribonucleic acid; tRNA, transfer ribonucleic acid; dsRNA, double-stranded ribonucleic acid; ssRNA, single-stranded ribonucleic acid; RNase, ribonuclease; NMR, nuclear magnetic resonance; TRIS, tris(hydroxymethyl)aminomethane; EDTA, ethylenediaminetetraacetic acid.

## REFERENCES

- (1) Zamani, F., Suzuki, T. (2021) Synthetic RNA Modulators in Drug Discovery, *J. Med. Chem.* 64, 7110–7155.
- (2) Baisden, J. T., Childs-Disney, J. L., Ryan, L. S., Disney, M. D. (2021) Affecting RNA Biology Genome-Wide by Binding Small Molecules and Chemically Induced Proximity, *Curr. Opin. Chem. Biol.* 62, 119–129.
- (3) Falese, J. P., Donlic, A., Hargrove, A. E. (2021) Targeting RNA with Small Molecules: From Fundamental Principles towards the Clinic, *Chem. Soc. Rev.* 50, 2224–2243.
- (4) Costales, M. G., Childs-Disney, J. L., Haniff, H. S. Disney, M. D. (2020) How We Think about Targeting RNA with Small Molecules, *J. Med. Chem.* 63, 8880–8900.
- (5) Giorgio, A. D., Duca, M. (2019) Synthetic Small-Molecule RNA Ligands: Future Prospects as Therapeutic Agents, *Med. Chem. Commun.* 10, 1242–1255.
- (6) Warner, K. D., Hajdin, C. E., Weeks, K. M. (2018) Principles for Targeting RNA with Drug-like Small Molecules, *Nat. Rev. Drug Discov.* 17, 547–558.
- (7) Connelly, C. M., Moon, M. H., Schneekloth, J. S. (2016) The Emerging Role of RNA as a Therapeutic Target for Small Molecules, *Cell Chem. Biol.* 23, 1077–1090.
- (8) Roberts, T. C., Langer, R., Wood, M. J. A. (2020) Advances in Oligonucleotide Drug Delivery, *Nat. Rev. Drug Discov.* 19, 673–694.
- (9) Bennett, C. F. (2019) Therapeutic Antisense Oligonucleotides Are Coming of Age, *Annu. Rev. Med.* 70, 307–321.
- (10) Chi, X., Gatti, P., Papoian, T. (2017) Safety of Antisense Oligonucleotide and siRNA-Based Therapeutics. *Drug Discov. Today* 22, 823–833.
- (11) Ratni, H., Scalco, R. S., Stephan, A. H. (2021) Risdiplam, the First Approved Small Molecule Splicing Modifier Drug as a Blueprint for Future Transformative Medicines. *ACS Med. Chem. Lett.* 12, 874–877.
- (12) Hargrove, A. E. (2020) Small Molecule–RNA Targeting: Starting with the Fundamentals, *Chem. Commun.* 56, 14744–14756.
- (13) Rizvi, N. F., Santa Maria, J. P., Nahvi, A., Klappenbach, J., Klein, D. J., Curran, P. J., Richards, M. P., Chamberlin, C., Saradjian, P., Burchard, J., Aguilar, R., Lee, J. T., Dandliker, P. J., Smith, G. F., Kutchukian, P., Nickbarg, E. B. (2020) Targeting RNA with Small Molecules: Identification of Selective, RNA-Binding Small Molecules Occupying Drug-Like Chemical Space, *SLAS Discov.* 25, 384–396.
- (14) Morgan, B. S., Forte, J. E., Culver, R. N., Zhang, Y., Hargrove, A. E. (2017) Discovery of Key Physicochemical, Structural, and Spatial Properties of RNA-Targeted Bioactive Ligands, *Angew. Chem. Int. Ed.* 56, 13498–13502.
- (15) Thomas, J. R., Liu, X., Hergenrother, P. J. (2005) Size-Specific Ligands for RNA Hairpin Loops, *J. Am. Chem. Soc.* 127, 12434–12435.
- (16) Thomas, J. R., Liu, X., Hergenrother, P. J. (2006) Biochemical and Thermodynamic Characterization of Compounds That Bind to RNA Hairpin Loops: Toward an Understanding of Selectivity, *Biochemistry* 45, 10928–10938.
- (17) Moumné, R., Larue, V., Seijo, B., Lecourt, T., Micouin, L., Tisné, C. (2010) Tether Influence on the Binding Properties of TRNAl<sub>ys3</sub> Ligands Designed by a Fragment-Based Approach, *Org. Biomol. Chem.* 8, 1154–1159.
- (18) Chung, F., Tisné, C., Lecourt, T., Dardel, F., Micouin, L. (2007) NMR-Guided Fragment-Based Approach for the Design of tRNA(Lys<sub>3</sub>) Ligands, *Angew. Chem. Int. Ed.* 46, 4489–4491.
- (19) Lee, M. M., Childs-Disney, J. L., Pushechnikov, A., French, J. M., Sobczak, K., Thornton, C. A., Disney, M. D. (2009) Controlling the Specificity of Modularly Assembled Small Molecules for RNA via Ligand Module Spacing: Targeting the RNAs That Cause Myotonic Muscular Dystrophy, *J. Am. Chem. Soc.* 131, 17464–17472.
- (20) Meyer, S. T., Hergenrother, P. J. (2009) Small Molecule Ligands for Bulged RNA Secondary Structures, *Org. Lett.* 11, 4052–4055.
- (21) Melidis, L.; Hill, H. J.; Coltman, N. J.; Davies, S. P.; Winczura, K.; Chauhan, T.; Craig, J. S.; Garai, A.; Hooper, C. A. J.; Egan, R. T.; McKeating, J. A.; Hodges, N. J.; Stamatakis, Z.; Grzechnik, P.; Hannon, M. J. Supramolecular Cylinders Target Bulge Structures in the 5' UTR of the RNA Genome of SARS-CoV-2 and Inhibit Viral Replication. *Angew. Chem.* 2021, 133, 18292–18299.
- (22) Phongtongpasuk, S., Paulus, S., Schnabl, J., Sigel, R. K. O., Spingler, B., Hannon, M. J., Freisinger, E. (2013) Binding of a Designed Anti-Cancer Drug to the Central Cavity of an RNA Three-Way Junction, *Angew. Chem. Int. Ed.* 52, 11513–11516.
- (23) Barros, S. A., Chenoweth, D. M. (2014) Recognition of Nucleic Acid Junctions Using Triptycene-Based Molecules, *Angew. Chem. Int. Ed.* 53, 13746–13750.

- (24) Barros, S. A., Yoon, I., Chenoweth, D. M. (2016) Modulation of the E. Coli RpoH Temperature Sensor with Triptycene-Based Small Molecules, *Angew. Chem. Int. Ed.* 55, 8258–8261.
- (25) Brown, C. J., Farthing, A. C. (1949) Preparation and Structure of Di- p -Xylylene, *Nature* 164, 915–916.
- (26) Hope, H., Bernstein, J., Trueblood, K. N. (1972) The Crystal and Molecular Structure of 1,1,2,2,9,9,10,10-Octafluoro-[2,2]Paracyclophane and a Reinvestigation of the Structure of [2,2]Paracyclophane, *Acta Cryst. B* 28, 1733–1743.
- (27) Hassan, Z., Spuling, E., Knoll, D. M., Lahann, J., Bräse, S. (2018) Planar Chiral [2.2]Paracyclophanes: From Synthetic Curiosity to Applications in Asymmetric Synthesis and Materials, *Chem. Soc. Rev.* 47, 6947–6963.
- (28) Brown J. A. (2020) Unraveling the structure and biological functions of RNA triple helices, *WIREs RNA* 11, e1598.
- (29) Sun, H., Tawa, G., Wallqvist A. (2012) Classification of scaffold-hopping approaches, *Drug. Discov. Today* 17, 310–324.
- (30) Kovalska, V. B., Kryvorotenko, D. V., Balanda, A. O., Losytskyy, M. Yu., Tokar, V. P., Yarmoluk, S. M. (2005) Fluorescent Homodimer Styrylcyanines: Synthesis and Spectral-Luminescent Studies in Nucleic Acids and Protein Complexes, *Dyes Pigm.* 67, 47–54.
- (31) Akbay, N., Losytskyy, M. Yu., Kovalska, V. B., Balanda, A. O., Yarmoluk, S. M. (2008) The Mechanism of Benzothiazole Styrylcyanine Dyes Binding with DsDNA: Studies by Spectral-Luminescent Methods, *J. Fluoresc.* 18, 139–147.
- (32) Zhu, C.-Q., Zhuo, S.-J., Zheng, H., Chen, J.-L., Li, D.-H., Li, S.-H., Xu, J.-G. (2004) Fluorescence Enhancement Method for the Determination of Nucleic Acids Using Cationic Cyanine as a Fluorescence Probe, *Analyst* 129, 254–258.
- (33) Felder, S., Micouin, L., Benedetti, E. (2021) Para-Functionalization of N-Substituted 4-Amino[2.2]Paracyclophanes by Regioselective Formylation, *Eur. J. Org. Chem.* 2021, 4015–4018.
- (34) Benedetti, E., Delcourt, M.-L., Gatin-Fraudet, B., Turcaud, S., Micouin, L. (2017) Synthesis and Photophysical Studies of Through-Space Conjugated [2.2]Paracyclophane-Based Naphthalene Fluorophores, *RSC Adv.* 7, 50472–50476.
- (35) Delcourt, M.-L., Reynaud, C., Turcaud, S., Favereau, L., Crassous, J., Micouin, L., Benedetti, E. (2019) 3D Coumarin Systems Based on [2.2]Paracyclophane: Synthesis, Spectroscopic Characterization, and Chiroptical Properties, *J. Org. Chem.* 84, 888–899.
- (36) Zeena, S., Thomas, K. G. (2001) Conformational Switching and Exciton Interactions in Hemicyanine-Based Bichromophores, *J. Am. Chem. Soc.* 123, 7859–7865. h
- (37) Zhai, D., Xu, W., Zhang, L., Chang, Y.-T. (2014) The Role of “Disaggregation” in Optical Probe Development, *Chem. Soc. Rev.* 43, 2402–2411.
- (38) Lee, J. C., Gutell, R. R. (2004) Diversity of Base-pair Conformations and their occurrence in rRNA structure and RNA structural motifs, *J. Mol. Biol.* 344, 1225–1249.
- (39) Wang, K.-N., Chao, X.-J., Liu, B., Zhou, D.-J., He, L., Zheng, X.-H., Cao, Q., Tan, C.-P., Zhang, C., Mao, Z.-W. (2018) Red Fluorescent Probes for Real-Time Imaging of the Cell Cycle by Dynamic Monitoring of the Nucleolus and Chromosome, *Chem. Commun.* 54, 2635–2638.
- (40) Tokar, V. P., Losytskyy, M. Yu., Ohulchanskyy, T. Y., Kryvorotenko, D. V., Kovalska, V. B., Balanda, A. O., Dmytruk, I. M., Prokopets, V. M., Yarmoluk, S. M., Yashchuk, V. M. (2010) Styryl Dyes as Two-Photon Excited Fluorescent Probes for DNA Detection and Two-Photon Laser Scanning Fluorescence Microscopy of Living Cells, *J. Fluoresc.* 20, 865–872.
- (41) Padroni, G., Patwardhan, N. N., Schapira, M., Hargrove, A. (2020) E. Systematic Analysis of the Interactions Driving Small Molecule–RNA Recognition, *RSC Med. Chem.* 11, 802–813.
- (42) Shelton, V. M., Sosnick, T. R., Pan T. (1999) Applicability of Urea in the Thermodynamic Analysis of Secondary and Tertiary RNA Folding, *Biochemistry* 38, 16831–16839.
- (43) Schweinefus, J. J., Kuprian, M. J., Lamma, J. W., Merker, W. E., Dorn, K. N., Muth, G. W. (2007) Human Telomerase RNA Pseudoknot and Hairpin Thermal Stability with Glycine Betaine and Urea: Preferential Interactions with RNA Secondary and Tertiary Structures, *Biochemistry* 46, 9068–9079.
- (44) Lambert, D., Draper, D. E. (2012) Denaturation of RNA Secondary and Tertiary Structure by Urea: Simple Unfolded State Models and Free Energy Parameters Account for Measured m-Values, *Biochemistry* 51, 9014–9026.
- (45) Feng, R., Li, L., Li, B., Li, J., Peng, D., Yu, Y., Mu, Q., Zhao, N., Yu, X., Wang, Z. (2018) A Small-Molecule with a Large Two-Photon Absorption Cross-Section Serves as a Membrane-Permeable Ribonucleic Acid (RNA) Probe for Live Cell Imaging, *New J. Chem.* 42, 14325–14331.
- (46) Dolomanov, O. V., Bourhis, L. J., Gildea, R. J., Howard, J. A. K., Puschmann, H. (2009) OLEX2: a complete structure solution, refinement and analysis program, *J. Appl. Cryst.* 42, 339–341
- (47) Sheldrick, G. M. (2015) SHELXT – Integrated space-group and crystal-structure determination, *Acta Cryst. A* 71, 3–8.
- (48) Sheldrick, G. M. (2015) Crystal structure refinement with SHELXL, *Acta Cryst. C* 71, 3–8.
- (49) Hibbert, D. B., Thordarson, P. (2016) The death of the Job plot, transparency, open science and online tools, uncertainty estimation methods and other developments in supramolecular chemistry data analysis, *Chem. Commun.* 52, 12792–12805.
- (50) Thordarson, P. (2011) Determining association constants from titration experiments in supramolecular chemistry, *Chem. Soc. Rev.* 40, 1305–1323.

Insert Table of Contents artwork here

